Inorg. Chem. **2007**, *46*, 4787–4789

Colloidal Unilamellar Layers of Tantalum Oxide with Open Channels

Katsutoshi Fukuda,[†] Izumi Nakai,[‡] Yasuo Ebina,[†] Renzhi Ma,[†] and Takayoshi Sasaki*,[†]

Nanoscale Materials Center, National Institute for Materials Science, 1-1 Namiki, Tsukuba, Ibaraki 305-0044, Japan, and Department of Applied Chemistry, Tokyo University of Science, 1-3 Kagurazaka, Shinjuku, Tokyo 162-8601, Japan

Received March 2, 2007

Layered tantalum oxide, $RbTaO_3$, was delaminated into colloidal TaO_3 unilamellar crystallites, which are characterized by an open-channel structure as well as a very small thickness of ~1.0 nm.

Functional nanosheet crystallites obtained via exfoliation of layered compounds have been widely investigated in the past decade because of their fundamental interest and technological relevance.[1−6] The nanosheets often exhibit distinctive physicochemical properties associated with extremely high two-dimensional anisotropy[7−10] and can be employed as a unique class of building blocks to fabricate diverse nanostructured materials. To achieve effective and rational design of nanostructures with nanosheets, it is essentially important to expand a library of nanosheets with a wide range of compositions, structures, and properties. For example, nanosheets with holes would lead to new functionalities and advantages because the diffusion of small molecules or ions through the sheet may be expected by such a "nanomesh" structure. The two-dimensional architectures of the nanosheets are sometimes disadvantageous in applications where efficient mass transportation in their stacked system is required. Here, we report that a nanosheet with open channels can be derived from the layered tantalum oxide, the host layer of which has holes of 1 × 1 width of a TaO_6 octahedron.

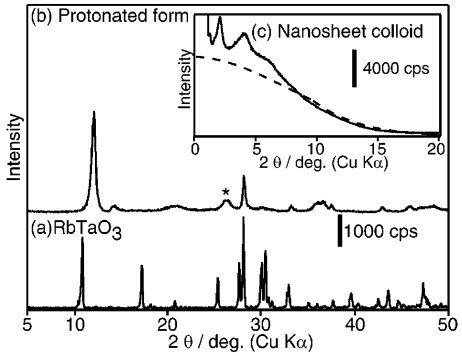

Figure 1. XRD patterns for (a) the starting material and (b) the protonated derivative. The inset (c) shows a X-ray halo from a nanosheet solid under a relative humidity of 95% (solid line) and a simulated pattern (broken line). A peak that could not be indexed is indicated by an asterisk.

X-ray diffraction (XRD) data of a hygroscopic powder obtained by heating a mixture of Rb_2CO_3 and Ta_2O_5 (see Figure 1a) could be readily indexed based on a C-base-centered monoclinic lattice. The pattern with indices can be found in Figure S1 in the Supporting Information. The refined unit cell dimensions, $a = 0.9587(4)$ nm, $b = 0.8508(4)$ nm, $c = 0.8133(3)$ nm, and $\beta = 94.37(2)°$, agree with those reported for the layered tantalum oxide, $RbTaO_3$.[11]

$RbTaO_3$ was reacted with a 1 mol dm^{-3} HCl solution for 3 days. The sample remained crystalline during the acid treatment, although some broadening of the diffraction peaks was observed (see Figure 1b). The basal 001 reflection was shifted to a higher angle of 12.1°, indicating an interlayer shrinkage of 0.08 nm. This shift may be understood by ion exchange from interlayer rubidium ions to protons or oxonium ions. The total pattern, except for a small peak at $2\theta = 26.6°$, could be indexed based on the same monoclinic symmetry with unit cell parameters of $a = 0.960(1)$ nm, b

* To whom correspondence should be addressed. E-mail: sasaki.takayoshi@nims.go.jp. Fax: +81-29-854-9061.
† National Institute for Materials Science.
‡ Tokyo University of Science.

(1) (a) Treacy, M. M.; Rice, S. B.; Jacobson, A. J.; Lewandowski, J. T. *Chem. Mater.* **1990**, *2*, 279. (b) Schaak, R. E.; Mallouk, T. E. *Chem. Mater.* **2002**, *14*, 1455.
(2) (a) Alberti, G.; Casciola, M.; Costantino, U. *J. Colloid Interface Sci.* **1985**, *107*, 256. (b) Kaschak, D. M.; Johnson, S. A.; Hooks, D. E.; Kim, H.-N.; Ward, M. D.; Mallouk, T. E. *J. Am. Chem. Soc.* **1998**, *120*, 10887.
(3) Schaak, R. E.; Mallouk, T. E. *Chem. Commun.* **2002**, 706.
(4) (a) Sasaki, T.; Watanabe, M.; Hashizume, H.; Yamada, H.; Nakazawa, H. *J. Am. Chem. Soc.* **1996**, *118*, 8329. (b) Sasaki, T.; Watanabe, M. *J. Am. Chem. Soc.* **1998**, *120*, 4682.
(5) (a) Liu, Z.-H.; Ooi, K.; Kanoh, H.; Tang, W.-P.; Tomida, T. *Langmuir* **2000**, *16*, 4154. (b) Omomo, Y.; Sasaki, T.; Wang, L. Z.; Watanabe, M. *J. Am. Chem. Soc.* **2003**, *125*, 3568.
(6) (a) Adachi-Pagano, M.; Forano, C.; Besse, J. *Chem. Commun.* **2000**, 91. (b) Hibino, T.; Jones, W. *J. Mater. Chem.* **2001**, *11*, 1321. (c) Li, L.; Ma, R.; Ebina, Y.; Iyi, N.; Sasaki, T. *Chem. Mater.* **2005**, *17*, 4386. (d) Liu, Z.; Ma, R.; Osada, M.; Iyi, N.; Ebina, Y.; Takada, K.; Sasaki, T. *J. Am. Chem. Soc.* **2006**, *128*, 4872.
(7) Sasaki, T.; Watanabe, M. *J. Phys. Chem. B* **1997**, *101*, 10159.
(8) Sakai, N.; Ebina, Y.; Takada, K.; Sasaki, T. *J. Phys. Chem. B* **2005**, *109*, 9651.
(9) Osada, M.; Ebina, Y.; Takada, K.; Sasaki, T. *Adv. Mater.* **2006**, *18*, 295.
(10) Osada, M.; Ebina, Y.; Funakubo, H.; Yokoyama, S.; Kiguchi, T.; Takada, K.; Sasaki, T. *Adv. Mater.* **2006**, *18*, 1023.

(11) $a = 0.985_9$ nm, $b = 0.850_5$ nm, $c = 0.813_5$ nm, $\beta = 94.8_7°$ (Serafin, M.; Hoppe, R. *Angew. Chem.* **1978**, *90*, 387).

10.1021/ic7004002 CCC: $37.00
Published on Web 05/11/2007

= 0.8426(5) nm, c = 0.733(2) nm, and β = 94.5(2)°. Chemical analysis revealed that about 90% of the rubidium ions was removed. No change in the chemical valence of the tantalum ions during the acid treatment was confirmed by XANES spectra (see Figure S2 in the Supporting Information). As a result, the protonic tantalum oxide can be formulated as $Rb_{0.1}H_{0.9}TaO_3 \cdot 1.3H_2O$.

The protonated sample was shaken with a tetrabutylammonium hydroxide (TBAOH) solution at ambient temperature for >2 weeks. The dose of TBAOH was adjusted to be the equivalent of the exchangeable protons in the oxide. A translucent suspension was obtained after separation of an unreacted residue in a small amount by mild centrifugation at 2000 rpm.

The dispersed material in the suspension could be totally sedimented by centrifugation at a higher speed of 10 000 rpm. XRD measurement under a relative humidity of 95% for the as-sedimented wet sample indicated that a drastic change occurred upon the treatment with TBA ions (Figure 1c), which involves the loss of the original basal reflections and the evolution of a broad profile. A major halolike pattern accompanied by sharp diffraction lines as a minor component has been observed for other exfoliated nanosheet systems, e.g., $Ti_{0.91}O_2$,[4b] MnO_2,[5b] $Ca_2Nb_3O_{10}$,[12] $Mg_{2/3}Al_{1/3}(OH)_2$,[6c] and $Co_{2/3}Al_{1/3}(OH)_2$.[6d] The broad pattern showed a characteristic profile depending on each nanosheet, which can be accounted for by the square of the structure factor with the scattering vector normal to each unilamellar sheet. On the other hand, the sharp peaks are attributable to the diffraction from sheets organized in parallel with a very large separation, which may be an initial stage of restacking promoted by drying. Thus, a structure factor $F_\perp(\theta)$ for the single host layer with a composition of TaO_3 was calculated by the following equation on the basis of its architecture illustrated in Figure 2a:

$$F_\perp(\theta) = \frac{1}{2}f_{Ta} + \frac{1}{2}f_{Ta}\cos[2\pi\{2 \times 0.158 \sin\theta/\lambda\}] + \frac{1}{2}f_O\cos[2\pi\{2 \times 0.040 \sin\theta/\lambda\}] + f_O\cos[2\pi\{2 \times 0.084 \sin\theta/\lambda\}] + f_O\cos[2\pi\{2 \times 0.170 \sin\theta/\lambda\}] + \frac{1}{2}f_O\cos[2\pi\{2 \times 0.332 \sin\theta/\lambda\}]$$

where f_{Ta} and f_O are the atomic scattering factors for tantalum and oxygen atoms and θ and λ are the diffraction angle and wavelength of the X-ray, respectively. The square of the calculated $F_\perp(\theta)$ designated by the broken line in Figure 1c is similar to the broad component. This close matching is clear evidence for the formation of TaO_3 nanosheet crystallites. A large majority of the sheet is not stacked to induce interference of the X-ray, but the sheets individually scatter the X-ray.

Transmission electron microscopy (TEM) observation visualized the morphology of the TaO_3 nanosheets. A typical image in Figure 3 shows two-dimensional sheets with very faint but uniform contrast. The lateral size was several hundreds of nanometers for the sample via exfoliation with a mechanical shaker. Larger sheets of up to a few micrometers were obtained when the delamination was carried out by gentle intermittent shaking by hand. The selected-area electron diffraction revealed a single-crystal pattern having sharp spots. The pattern can be indexed as a face-centered rectangular unit cell (0.98 nm × 0.87 nm), being consistent with the two-dimensional symmetry of the parent host layer.

This was corroborated by an in-plane XRD pattern for a self-assembled film (see Figure 4), in which the TaO_3 nanosheets lie flat to the substrate in the monolayer.[13] All of the reflections in the 1/d region from 1.8 to 8.7 nm^{-1} can

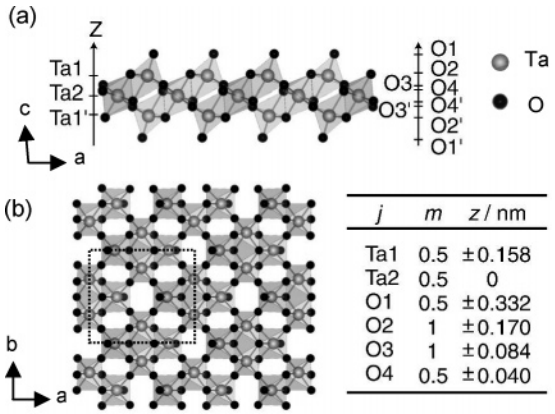

j	m	z / nm
Ta1	0.5	±0.158
Ta2	0.5	0
O1	0.5	±0.332
O2	1	±0.170
O3	1	±0.084
O4	0.5	±0.040

Figure 2. Crystal structure of the TaO_3 host layer projected along (a) the b^* axis and (b) the c^* axis. The broken line shows a two-dimensional unit cell. The relative distance, z, and site multiplicity, m, for the jth atom are listed in the right panel.

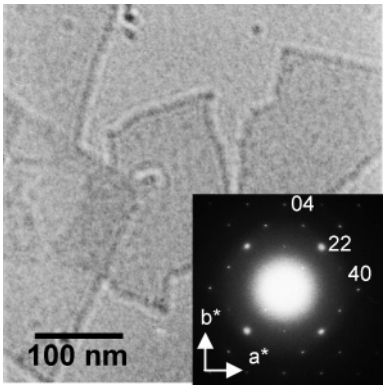

Figure 3. TEM micrograph of the TaO_3 nanosheets dropped on a copper grid and the selected-area electron diffraction pattern from a single nanosheet.

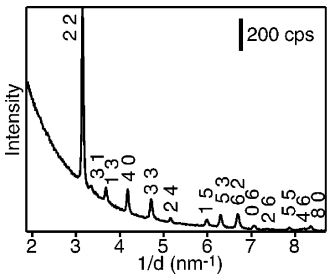

Figure 4. Synchrotron radiation in-plane XRD pattern for the monolayer film of the TaO_3 nanosheets. The indices with $h + k = 2n$ indicate the face-centered structure.

(12) Ebina, Y.; Sasaki, T.; Watanabe, M. *Solid State Ionics* **2002**, *151*, 177.
(13) Sasaki, T.; Ebina, Y.; Watanabe, M.; Decher, G. *Chem. Commun.* **2000**, 2163.

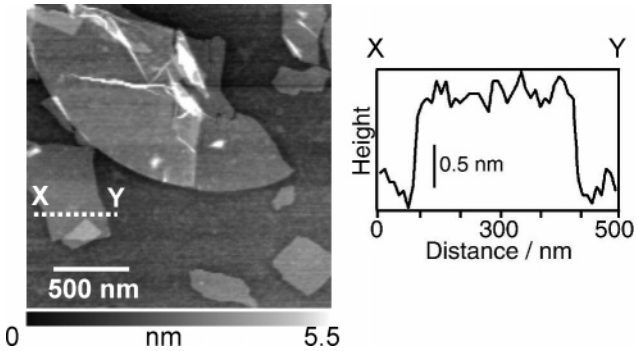

Figure 5. AFM image of the TaO_3 nanosheets. The right panel shows a height profile along the broken line.

also be indexed to yield refined unit cell parameters, $a = 0.9567(1)$ nm and $b = 0.8490(2)$ nm. These values are very similar to those of the precursors such as $RbTaO_3$ and its protonic form. Besides those, the intensity of each diffraction peak is substantially consistent with a square of the calculated structure factor for the parent host layer (see Figures 2b and S3 in the Supporting Information). These diffraction studies definitely indicate that the two-dimensional atomic arrangement in the original $RbTaO_3$, or the 1×1 mesh structure, was preserved after delamination.

The atomic force microscopy (AFM) image of the TaO_3 nanosheets adsorbed on a silicon substrate exhibited a number of sheets with a thickness of 1.03 ± 0.05 nm and a lateral size ranging from sub-micrometer to micrometers, as shown in Figure 5. The average thickness is compatible with that of the host layer deduced from the crystallographic data of $RbTaO_3$; the vertical distance between the levels of upper and bottom oxygen atoms (O1 and O1′ in Figure 2a) of the host layer is 0.66 nm, and summing up the ionic radius of these two oxygen atoms (0.28 nm) gives 0.94 nm. This good agreement further supports the unilamellar nature of the crystallites.

As demonstrated by the characterizations above, the TaO_3 nanosheets obtained in this study possess two kinds of holes regularly arranged in the sheet. Based on the crystallographic data of the parent host layer, the free open space of each hole excluding the ionic radius of the oxygen atoms can be calculated as 0.13×0.06 and 0.11×0.11 nm^2. The size of the holes is likely to allow the diffusion of alkali-metal ions smaller than sodium ions. This is considered to be a new feature of the exfoliated nanosheets, which may be useful for some applications such as nanocoating of solid electrolytes.

Figure 6 depicts a UV−vis absorption spectrum for the colloidal suspension of the TaO_3 nanosheets. The TaO_3 nanosheet exhibits intense absorption of UV light at a wavelength of 250 nm and below. The molar extinction coefficient was 1.15×10^4 mol^{-1} dm^3 cm^{-1} at 200 nm. The square of the absorption coefficient, α, times the photon energy, $h\nu$, is plotted against the photon energy. The upsurge

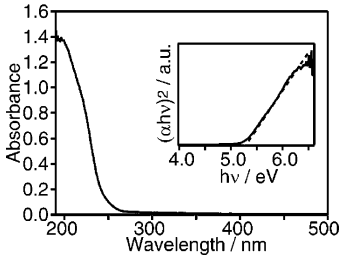

Figure 6. UV−vis absorption spectra for the colloidal suspension of the TaO_3 nanosheets (0.03 g dm^{-3}). The inset shows a plot of $(\alpha h\nu)^2$ vs $h\nu$.

portion of $(\alpha h\nu)^2$ can be fitted by the straight broken line. This proportional relationship suggests that the TaO_3 nanosheet has a direct electronic transition near the band gap. The optical bandgap energy for the TaO_3 nanosheets can be derived as about 5.3 eV at the intersection of the broken line and the abscissa. This value is larger than that of bulk Ta_2O_5, about 4 eV,[14] as a common tantalum(V) oxide. This may be attributable to the size quantization effects, as has been demonstrated for a titania nanosheet.[7,15] Thus, the TaO_3 nanosheets can be described as a new semiconductor nanomaterial with a wide bandgap.

It has been reported that some tantalum oxides are promising in their application as ferroelectrics.[16] Among them, $RbTaO_3$ is attractive because of its high ferroelectric performance and moderate T_c.[16c] Thus, the evaluation of such a property for the TaO_3 nanosheet would be intriguing. Realization of ferroelectric nanosheets with the thickness of ~1 nm will answer the increasing demand on thin ferroelectrics for downsizing of the electronic device. Such a study is now underway.

In conclusion, we have demonstrated that the tantalum oxide nanosheet having open channels was successfully obtained via the soft-chemical delamination of the layered tantalum oxide of $RbTaO_3$. The resulting unilamellar crystallites may be useful in a range of applications, e.g., nanoscale separators of lithium ion secondary batteries and ferroelectric materials.

Acknowledgment. This work was financially supported by CREST of Japan Science and Technology Agency.

Supporting Information Available: Experimental procedures and listings of figures (XRD patterns, XANES spectra, and calculated structure factors). This material is available free of charge via the Internet at http://pubs.acs.org.

IC7004002

(14) (a) Thomas, J. H., III. *J. Appl. Phys.* **1974**, *45*, 835. (b) Chu, K.; Chang, J. P.; Steigerwald, M. L.; Fleming, R. M.; Opila, R. L.; Lang, D. V.; Van Dover, R. B.; Jones, C. D. W. *J. Appl. Phys.* **2002**, *91*, 308.
(15) Sakai, N.; Ebina, Y.; Takada, K.; Sasaki, T. *J. Am. Chem. Soc.* **2004**, *126*, 5851.
(16) (a) Lines, M. E. *Phys. Rev. B* **1970**, *2*, 698. (b) Paz de Araujo, C. A.; Cuchiaro, J. D.; McMillan, L. D.; Scott, M. C.; Scott, J. F. *Nature* **1995**, *374*, 627. (c) Subbarao, E. C. *Ferroelectrics* **1973**, *5*, 267.